3D Bulk Ordering in Macroscopic Solid Opaline Films by Edge-Induced Rotational Shearing

Finlayson, Christopher Edward; Spahn, Peter; Snoswell, David R. E.; Yates, Gabrielle; Kontogeorgos, Andreas; Haines, Andrew I.; Hellmann, G. Peter; Baumberg, Jeremy J.

Published in:
Advanced Materials

DOI:
10.1002/adma.201003934

Publication date:
2011

Citation for published version (APA):
Finlayson, C. E., Spahn, P., Snoswell, D. R. E., Yates, G., Kontogeorgos, A., Haines, A. I., Hellmann, G. P., & Baumberg, J. J. (2011). 3D Bulk Ordering in Macroscopic Solid Opaline Films by Edge-Induced Rotational Shearing. *Advanced Materials*, *23*(13), 1540-1544. https://doi.org/10.1002/adma.201003934

Submitted to ADVANCED MATERIALS
DOI: 10.1002/adma.((please add manuscript number))

3D bulk-ordering in macroscopic solid opaline films by edge-shearing

By *C.E. Finlayson,* P. Spahn, D.R.E. Snoswell, G. Yates, A. Kontogeorgos, A.I. Haines, G.P. Hellmann, and J.J. Baumberg**

[*] Dr C.E. Finlayson, Dr D.R.E. Snoswell, G. Yates, A. Kontogeorgos, A.I. Haines, Prof. J.J. Baumberg
NanoPhotonics Centre,
University of Cambridge,
Cambridge CB3 0HE,
United Kingdom
E-mail: (cef26@cam.ac.uk, jjb12@cam.ac.uk)

Dr P. Spahn, Dr G.P. Hellmann
Deutsches Kunststoff-Institut (DKI),
Schlossgartenstrasse 6,
D-64289 Darmstadt,
Germany

Keywords: Opals, Self-assembly, Colloids, Photonic Crystals, Structural Color.

We report a significant breakthrough in the field of large area photonic structures, based on permanently ordering colloidal sub-micron polymeric spheres by edge-shearing. Transmission optical diffraction experiments demonstrate how we reach the important milestone of bulk 3D ordering in polymer photonic crystals. The resulting high-quality polymer opal thin-films exhibit strikingly intense structural color, as confirmed by combining a number of spectroscopic approaches, which is tuneable across visible wavelengths. This induced self-assembly on macroscopic length scales represents a step-change away from current surface lithographies, and presents a new paradigm for assembling ordered photonic materials. Whilst the effect of edge-shearing upon the ordering in colloidal ensembles has been previously reported,[1,2] no precedents exist for the application of such techniques to solvent-free granular systems, forming permanent composite structures in the solid-state. Reproducible mass-production of single-domain opals opens wide opportunities for applications such as sensors, indicators and coatings.

Full 3D ordering of sub-micron components into defined architectures is a major challenge for bottom-up nano-photonics, nano-electronics, plasmonics and metamaterials.[3-7] Even simple structures such as opaline photonic crystals based on *fcc* colloidal lattices have optical properties dominated by defects and cannot be fabricated in any scalable fashion.[8-10] Sedimentation or centrifugal-based processes are too slow or defective, while the best shear-assembly processed films so far exhibit scattering-dominated structural colour.[11] Here we report a significant advance in high-quality polymer opal thin-films exhibiting tuneable structural colour across visible wavelengths. An edge-shearing process produces reproducible highly-uniform samples with bulk-ordering of sub-micron components, greatly enhancing both the intensity and chromaticity of the observed structural colour. Demonstrating scale-up of these synthetic opaline films to industrial length scales makes them very attractive as a route to a wide range of large-area photonics applications, including sensors and coatings.[12]

A promising cost-effective, large-scale technique to produce flexible opals has recently been developed using melting and shear-ordering under compression of core/shell polymer nanoparticles.[13-15] So far, this produces low-defect single-domain flexible polymer opals with fundamental optical resonances tuneable across the visible and near-infrared regions (by varying the precursor nano-sphere size from 200-350nm, and hence the resulting *fcc* lattice parameter). In the low refractive-index contrast regime associated with these polymer composites, colour generation arises through spectrally-resonant scattering inside a 3D *fcc*-lattice photonic crystal,[16] as opposed to normal reflective iridescence based on Bragg diffraction. This principle is of fundamental interest in understanding the origins of structural colors and iridescence in natural opals, such as those in minerals or in biological structures.[17] In addition, one of the most attractive features (and applications) of elastomeric polymer opals is the tunability of their perceived color by the bending or stretch modification of the (111) plane spacing. However the main difficulty of this fabrication approach has been the lack of true bulk order, and it is this advance that is reported below.

The polymeric opal system described in this paper is based on ensembles of core-interlayer-shell (CIS) particles, synthesized by an emulsion polymerisation process, as previously reported.[18,19] Rigid cross-linked polystyrene spheres are capped by a soft poly-ethylacrylate (PEA) shell, via a poly-methylmethacrylate (PMMA) grafting layer (**Fig.1a**). The net refractive index contrast between core and shell material is $\Delta n/n \approx 0.11$. A full description of the process, which consists of a combination of rolling (linear shear) and edge shearing processes, yielding permanent rolls of opal films (**Fig.1b**), is given in the *Experimental* section. This edge-shear step may be done as a single-pass or may be repeated several times in either direction. The resultant opaline samples are observed to have a brilliant visual iridescence (**Figs.1e-h**), which markedly improves during the edge-shear step. These images also illustrate how this iridescence is readily tuneable, both with the size and spacing of the core particles (the green opal has a base core diameter of ~215 nm with a spacing of ~275 nm; for the red opal, these values are 250 nm and 310 nm respectively), and also with the angle of viewing. Edge-shear induces ensembles of the CIS polymer particles to form highly-ordered opaline structures under the melt conditions at 150˚C (**Fig. 1d**), which this paper aims to characterise and understand.

A spectroscopic study of typical green opal samples shows a clear enhancement of both bright- and dark-field reflectance after edge-shearing (**Fig.2**). For consistency we concentrate below on green opal films with 0.05wt% carbon nanoparticle loading, unless otherwise stated. In such a photonic crystal medium of relatively low refractive index contrast, resonant back scattering (in dark-field) is seen to be greater than the normal incidence reflection (bright-field). Plotting the chromaticity of reflected light from green opal samples (supplementary information, **Fig. S1**) on the *Commission Internationale de l'Eclairage* (CIE) color space shows that the edge-shearing process produces near-saturated colours (of 20nm linewidth, black dashed line, compared to pure monochromes at the CIE edge) from the initial

samples of near white chromaticity (at the CIE centre). This enhancement in perceived color is also vividly demonstrated in the images in **Fig.2a** (inset).

Whilst the reflectivity spectra imply opaline ordering within the optical depth of the samples, typically <20μm,[16] a better indication of bulk ordering is given by the optical transmittance spectra (**Fig.2b**). Before edge-shearing we observe a featureless spectrum characterised by decreasing transmittance at short wavelengths, as expected from an ensemble of scattering centres with poor structural ordering.[20] Visually, such samples appear dark orange in transmitted light, with little or no variation with viewing angle. There is a dramatic change after the edge-shearing process with a pronounced minimum in the transmission spectrum corresponding to the resonant wavelength of a bulk-ordered array of scatterers, the width of this resonance being determined by the resultant photonic stopband. Commensurately, the edge-sheared samples show a very marked visual *complementary color* effect when viewed in transmission, which is also strongly tuneable with viewing angle (Fig.2b, inset).

Lateral cross sections of the films taken at 30° to the shear-direction show near-resonant (111)-plane optical scattering allowing study of ordering at different depths within the films (supplementary information, **Fig. S2**). Previous compression processing of opal thin-films from the as-extruded CIS bulk material via squeeze-shear[15,16] had the drawback that the opals tend to be formed of discrete well-ordered surface layers and a poorly-ordered interior (Fig. S2c). Hence these previous samples show weaker structural color and virtually no effect in transmittance due to the lack of uniform bulk-ordering. By contrast, cross-sectional dark-field images of the current samples (Figs. S2a-b) already show no obvious signs of any layering after the first linear shear process. Dark- and bright-field spectra taken across the thickness profile of the samples are found to be virtually independent of position. Hence, the uniformity present in the sample before the edge-shearing process is also maintained in the final highly-ordered sample.

As a vivid demonstration of the exceptional 3D bulk ordering that may be achieved in these opaline films, optical diffraction experiments were performed on films in transmittance. For samples where the core spacing of the opal was of the same order of the λ = 404 nm laser source, this readily revealed very clear and distinctive diffraction patterns, with a characteristic six-fold symmetry (**Fig. 3a-b**). In-plane rotation of the sample, normal to the incident beam, produced the expected co-rotation of the diffraction pattern. Based upon the measured angle of diffraction of 54˚, the fcc-lattice spacing of the (111) plane was calculated to be around 500 nm, in good agreement with expectation for spheres of spacing ~680 nm. The interpretations of these experiments are two-fold; firstly, the appearance of such well resolved diffraction spots for the edge-sheared sample represents clear evidence of a mono-domain crystalline structure within the film. We believe that the broadening of these spots relates mainly to the finite particle size, relative to the lattice spacing.[21] Secondly, a significant sharpening of the diffraction spots was also noted, when comparing an edge-sheared sample to one which had not been. This gives a further indication of the improved ordering following the edge-shearing process.

To better understand the role of edge-shearing on the ordering within the polymer opal system, we consider the motion of sub-volumes within the film (of initial thickness *t*) which are rigidly stuck to the outer PET sheets (**Fig.3c**). This model shows how the bending of the opal at the hot-edge (apex angle α = 90˚ and radius of curvature <10μm) produces a *vertical* shear strain, σ_v, (as opposed to the applied lateral shear strain, $\sigma_h = \alpha$ in radians), whose orientation rotates as the sub-volumes follow the top and bottom sheets. From the net shear of the films relative to each other over the bending edge, we predict a thinning of the opal film, depending upon the bending angle after the film relaxes, θ. This thinning is revealed by measuring the cross-section of an opal film parallel to the processing direction (**Fig.3d**) which has been stopped with the hot-edge at the point indicated. The thinning profile indeed resembles the model in Fig.3c, and the thickness of the opal film decreases by $\Delta t/t$ = 9%. We

note that in the ideal case, the lateral shear would produce a thinning $\Delta t/t = 1\text{-}\cos[\tan^{-1}(\alpha)] =$ 47%, hence there is currently a degree of slip within the apparatus. The measured thinning corresponds to a bending angle $\theta = \cos^{-1}(1\text{-}\Delta t/t) = 24^\circ$ and a net vertical strain of $\sigma_v = \tan(\theta) =$ 46%. This level of strain in the sample is significant, as it exceeds the critical yield strain beyond which the lattice planes in the opal are found to start slipping past each other, at 25% shear strain.[15] This observed yield strain is in good agreement with that expected for a perfect *fcc* hard-sphere model.[22,23] Previous optical surface-diffraction measurements have shown that the shear-processing direction completely sets the [110] close-packed orientation of the hexagonal lattice,[14,23] with the (111) plane remaining parallel to the top sample surface despite the rotating vertical shear. We also observe up to 3% red-shift of the Bragg peak after several passes (Fig.2a). Within the visco-elastic regime of the CIS ensemble, such a slipping and relaxation process provides a mechanism for the core particles to be reconfigured towards a fully crystalline ordering. The role of the edge-shear geometry is to provide a controllable *fixed* shear strain (but not shear flow) for each point in the film, as we previously showed is critical for ordering.[15] We suggest that shear strains of 40% favour the *fcc* lattice by concentrating shear forces along close packed directions towards the walls: defects in these close-packed directions (from domains of hexagonal- or random-close packing) yield first, selectively annealing them out and providing a mechanism for beyond nearest-neighbour hard-sphere interactions (Monte-Carlo simulations underway aim to confirm this hypothesis). Controlling the shear strain using the hot edge process has the advantage that the rate of shearing can be kept well below the threshold for shear melting[15] above which all sample properties rapidly degrade. As a further confirmation of the edge-shear mechanism, concentric holes made through the top and bottom PET films showed a relative motion of x = 20-30 μm after the samples had been processed, consistent with the shear-angle extracted from the above model.

To map the regime of edge-shear in ordering these polymer opal thin films, the effects of multiple-pass edge-shear processing and variation with processing speed on the spectra are investigated (Fig.2c). The depth of the resonant minimum in transmittance is parameterized as Q, given by the difference between the dip intensity and the shorter-wavelength transmission (Fig.2c, inset). This quality parameter of 3D order is seen to significantly improve, not only after the first-pass of edge-shear, but also with subsequent repeat passes at a speed of 5mm s^{-1}. By comparison, the intensity and full-width-half-maximum (FWHM) of the bright- and dark-field reflectance spectra improve markedly after the first-pass edge-shear (supplementary information, **Fig.S3**), but do not significantly improve with subsequent passes. These results indicate that, remarkably, the surface-ordering in the opal goes to near-completion on a *single-pass* of the hot-edge, whereas the bulk-ordering may still be improved upon by repeated processing. To reconcile these observations, bright-field reflectance of the top and bottom surfaces is compared for increasing hot-edge passes (Fig.2d). After the linear shear (rolling) process, the bottom surface appears slightly more ordered than the top surface. However, a single pass of the hot-edge produces a much stronger structural color effect on the top surface than the bottom; we believe this is because the shearing forces are not uniform throughout the film, but are greatest on the top surface, which is furthest from the point of the hot-edge apex. Successive repeat passes then cause this color to improve on both sides, culminating in the top/bottom spectra being virtually identical after three passes. This confirms the progressive improvement in bulk-ordering across the full depth of the film upon repeated edge-shearing. While the quality $Q \approx 0.1$ for processing speeds of 2, 5 and 10 mm s^{-1} (Fig. S3), it rapidly degrades for the broad spectra measured at speeds exceeding 20 mm s^{-1}. Although structural color in surface reflectance is still present for faster processing speeds, the dynamics of shearing is too slow to develop full bulk-ordering in ~100 mm thick films at these processing temperatures.

We anticipate being able to extend the paradigms described here into a much wider range of CIS systems, using polymers and polymeric composites. For example, work currently in progress modifies the composition of the interlayer and shell components, to tune the refractive contrast of such polymeric opals.[24] Synthetic opals or inverse opal structures, with strong structural color effects can be used as a replacement for toxic and carcinogenic dyes and pigments. However many reported structures[3-11] based on self-assembly or microfabrication suffer from poor lattice quality due to cracks and polycrystallinity, poor mechanical robustness, and are difficulty to scale processing up to macroscopic dimensions, all of which limit the practical structural color applications. The novel use of soft nanomaterials in the design of photonic structures, with macroscale bulk-ordering, presents opportunities for a step-change away from the monolithic architectures which are currently relied upon, with the goal of key advances in the areas of organic optoelectronics and optical metamaterials. The unique structural colour properties of polymeric opals, together with intrinsic processability, stretchability and durability also make them attractive for mainstream applications, such as decorative coatings, security/anti-forgery labelling and in thermochromic indicators.[24]

Experimental

Sample Preparation: As-synthesized batches of the CIS material, together with a small amount (<0.1% by weight) of a scattering pigment such as carbon black or a black pigment dye, are extruded into mm-sized ribbons using a twin co-rotating-screw mini-extruder at 150˚C. In order to produce thin-film opaline samples, these ribbons are then encapsulated between 2 metre-long, 4 cm wide polyester (PET) tapes, as illustrated in Figs.1(b,c). The tapes are fed under a quartz roller, which has a compressive downwards pressure of 40 psi, and through a cartridge consisting of a polished brass hot-edge, with an apex angle of $\alpha = 90^{\circ}$

and radius of curvature <10μm. The sample is positioned on a heated glass plate, with the cartridge and plate being pre-heated to 150˚C. Firstly, the translation stage is moved horizontally at 1 mm s^{-1} relative to the roller, which is free to rotate, pressing the sample into uniform thin films in a squeeze/shear mechanism (Fig.1c). The roller is typically set to produce thicknesses of order 100 μm and films of area 10-20 cm^2. Secondly, the PET tapes are secured at both ends and the translation stage is used to draw the thin-film tapes over the heated brass edge at typical speeds of 5 mm s^{-1}. This latter step may be done as a single-pass or may be repeated several times in either direction.

Diffraction Experiments: The beam from a Coherent CUBE laser (λ = 404 nm) was down-sized to a circular diameter of ~0.5 mm using an iris. The opaline samples were carefully mounted as free-standing films, illuminated with a few mW of laser power, and the diffracted patterns in transmission were projected at normal incidence onto a white card at a distance of several centimetres. The positions of spots and rings were accurately marked out and images were recorded using a digital camera. The samples were mounted in such a way as to enable in-plane rotation, normal to the incident beam.

Spectroscopy: All spectroscopic measurements reported were taken with an adapted Olympus BX51 microscope, using a focused spot size of approximately 2×2 μm (×20 magnification), with the light signal collected using suitable focusing optics and a fibre-coupled CCD spectrometer. The spectra were standardised using a highly-reflective aluminium mirror (bright-field reflectance), a diffusive white-light scatterer (dark-field reflectance) and by using appropriate control films of the PET encapsulant (transmittance).

Microscopy: Thin-films were cross-sectioned for microscopy by carefully placing samples in molten dental wax and then setting to hardness by cooling with liquid nitrogen. Thin microtomes of the sample were then removed with a micro-positioned glass knife-edge, at room temperature, until a suitably clean cross-section of the film was visible at the surface of

the wax. All the microscopic images displayed were then taken with an Olympus BX51 light microscope.

Acknowledgements
This work was supported by EPSRC (UK) grants EP/G060649/1, EP/E040241. The authors thank Prof. M. Mackley of the University of Cambridge for very helpful discussions and R. Hardy of the Cavendish Laboratory for technical assistance.

Received: ((will be filled in by the editorial staff))
Revised: ((will be filled in by the editorial staff))
Published online: ((will be filled in by the editorial staff))

[1] B. J. Ackerson, P. N. Pusey, *Phys. Rev. Lett.* **1988**, *61*, 1033.

[2] R. M. Amos, J. G. Rarity, P. R. Tapster, T. J. Shepherd, *Phys. Rev. E* **2000**, *61*, 2929.

[3] R. de la Rue, *Nature Mater.* **2003**, *2*, 74.

[4] S. G. Johnson, J. D. Joannopoulos, in *Photonic Crystals; the Road from Theory to Practice* (Kluwer Academic, Dordrecht, **2003**)

[5] Y. A. Vlasov, X. Z. Bo, J. C. Sturm, D. J. Norris, *Nature* **2001**, *414*, 289.

[6] D. N. Sharp, A. J. Turberfield, R. G. Denning, *Phys. Rev. B* **2003**, *68*, 205102.

[7] P. Nagpal, N.C. Lindquist, S-H. Oh, D. J. Norris, *Science* **2009**, 31, 594.

[8] V. N. Astratov, A. M. Adawi,S. Fricker, M. S. Skolnick, D. M. Whittaker, P. N. Pusey, *Phys. Rev. B* **2002**, *66*, 165215.

[9] A. A. Chabanov, Y. Jun, D. J. Norris, *Appl. Phys. Lett.* **2004**, *84*, 3573.

[10] A. F. Koenderink, A. Lagendijk, W. L. Vos, *Phys. Rev. B* **2005**, *72*, 153102.

[11.] S. A. Asher, J. M. Weissman, A. Tikhonov, R. D. Coalson, R. Kesavamoorthy, *Phys. Rev. B* **2004**, *69*, 066619.

[12] J. Ge, Y. Hu, Y. Yin, *Angew. Chem. Int. Ed.* **2007**, *46*, 7428.

[13] O. L. J. Pursiainen, J. J. Baumberg, H. Winkler, B. Viel, T. Ruhl, *Appl. Phys. Lett.* **2005**, *87*, 101902.

[14] O. L. J. Pursiainen, J. J. Baumberg, H. Winkler, B. Viel, P. Spahn, T. Ruhl, *Adv Mater.* **2008**, *20*, 1484.

[15] D. R. E. Snoswell, A. Kontogeorgos, J. J. Baumberg, T. D. Lord, M. R. Mackley, P. Spahn, G. P. Hellmann, *Phys. Rev. E* **2010**, *81*, 020401.

[16] O. L. J. Pursiainen, J. J. Baumberg, H. Winkler, B. Viel, P. Spahn, T. Ruhl, *Opt. Express* **2007**, *15*, 9552.

[17] P. Vukusic, J. R. Sambles, *Nature* **2003**, *424*, 852.

[18] T. Ruhl, P. Spahn, G. P. Hellmann, *Polymer* **2003**, *44*, 7625.

[19] B. Viel, T. Ruhl, G. P. Hellmann, *Chem. Mater.* **2007**, 19, 5673.

[20] P. Ossi, in *Disordered Materials* (Springer-Verlag, Heidelberg, Germany, **2006**).

[21] M. D. Haw, W. C. K. Poon, P. N. Pusey, *Phys. Rev. E* **1998**, *57*, 6859.

[22] R. Abbaschian, R. E. Reed-Hill, in *Physical Metallurgy Principles* (CL-Engineering, **2008**).

[23] A. Kontogeorgos, D. R. E. Snoswell, C. E. Finlayson, J. J. Baumberg, P. Spahn, G. P. Hellmann, submitted **2010**.

[24] J. Sussman, D. R. E. Snoswell, A. Kontogeorgos, J. J. Baumberg, P. Spahn, *Appl. Phys. Lett*. **2009**, *95*, 173116.

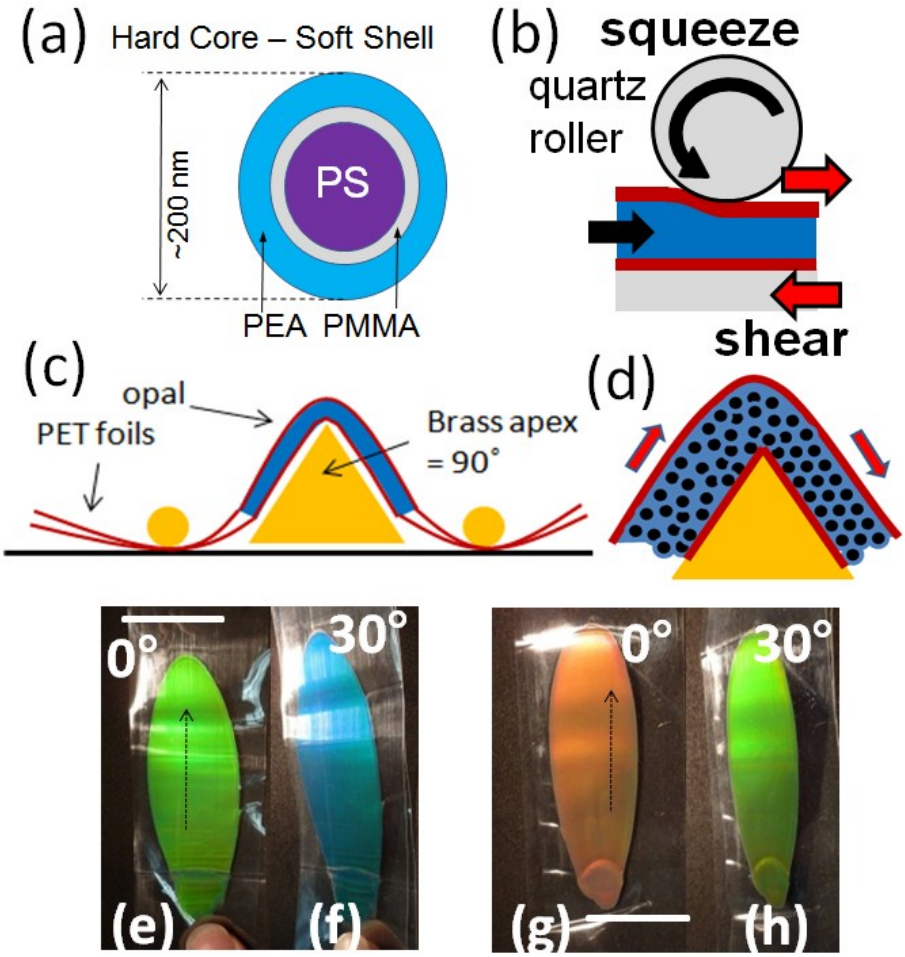

Figure 1. (a) Core-interlayer-shell (CIS) of the constituent particles used in polymer opals. (b) schematic of the roller process producing 100µm-thick opal films via squeeze/linear-shear. (c) schematic of hot-edge process, exploiting edge-shearing mechanism as illustrated in (d). (e,f) Photos of a processed green opal sample viewed in reflected white-light at angles of (e) 0˚ and (f) 30˚ to the normal. (g,h) Corresponding images of a red opal sample. Arrows in (e,g) show direction of edge-shear processing, scale bars are 3 cm.

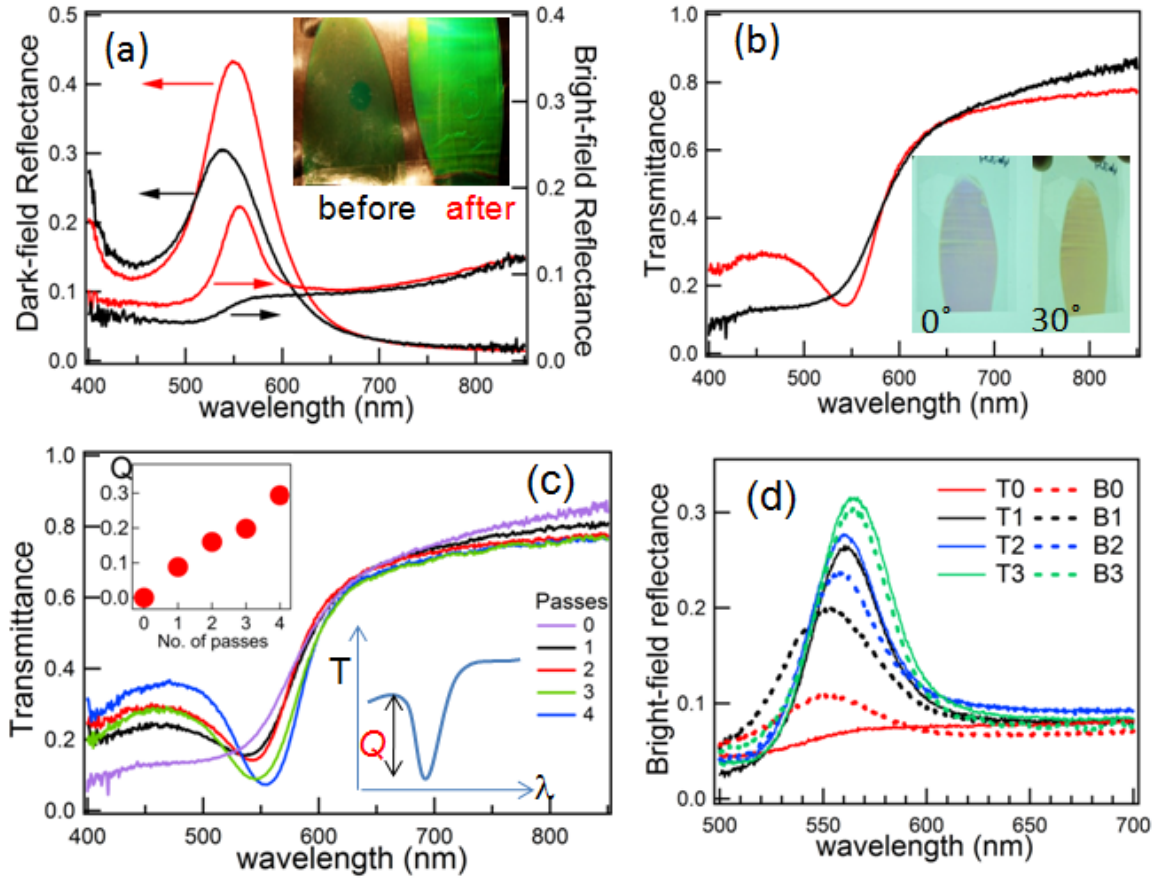

Figure 2. (a) Dark- and bright-field normal incidence reflectivity for a green opal thin-film before (black) and after (red) a single-pass edge-shear. Inset; raw photos in reflected white-light of the edge-sheared opal film (right) and the pre-sheared film (left). (b) Transmission spectra for 100μm thick films. Inset; photo with white-light back-illumination of edge-sheared opal film, viewed at 0˚ (left) and 30˚ (right) to the normal. (c) Transmission spectrum of green opaline films as a function of the number of edge-shearing passes at 5 mm s^{-1}, compared to a 100mm thick film before shearing. Insets; sample quality, *Q*, (see text) vs number of passes. (d) bright-field reflectance spectra of the top (T) and bottom (B) surfaces, as the number of passes is increased.

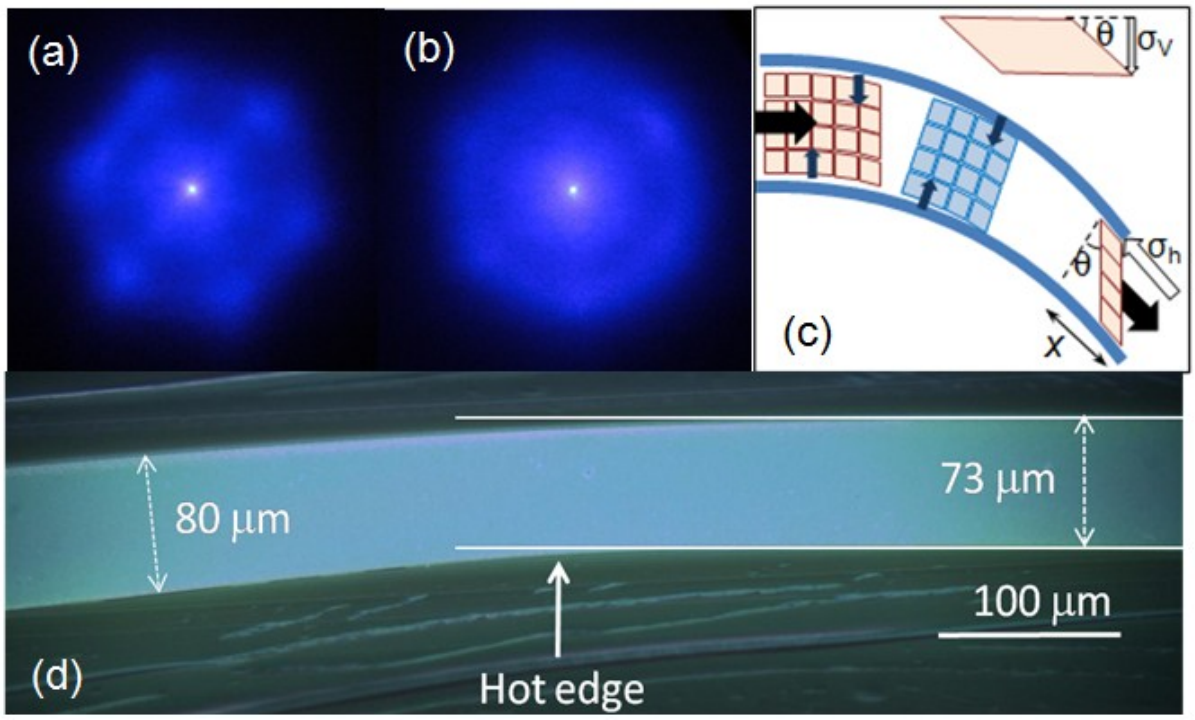

Figure 3. (a,b) Transmission diffraction patterns taken at normal incidence for ~40 μm thick films of an opal with sphere diameter 630 nm. A clear difference in the pattern can be seen between films with (a) and without (b) edge-shearing. (c) Schematic of bend-induced shearing (blue arrows) of opal between rigid PET films passed over edge, developing horizontal shear strain (σ_h) and vertical shear strain (σ_v, upper inset) perpendicular to processing direction. (d) Microscope image (x20, dark-field) of green-opal film in cross-section transverse to the edge-shear processing direction, during edge-shear process (edge stopped at point indicated).

The table of contents entry

A significant breakthrough in the field of large area photonic structures is reported, based on permanently ordering colloidal sub-micron polymeric spheres by edge-shearing. Transmission optical diffraction experiments demonstrate an important milestone of bulk 3D ordering in polymer photonic crystals. The resulting high-quality polymer opal thin-films exhibit strikingly intense tuneable structural color.

Keyword; 3D photonic crystals

C.E. Finlayson,* P. Spahn, D.R.E. Snoswell, G. Yates, A. Kontogeorgos, A.I. Haines, G.P. Hellmann, and J.J. Baumberg*

3D bulk-ordering in macroscopic solid opaline films by edge-shearing

ToC figure

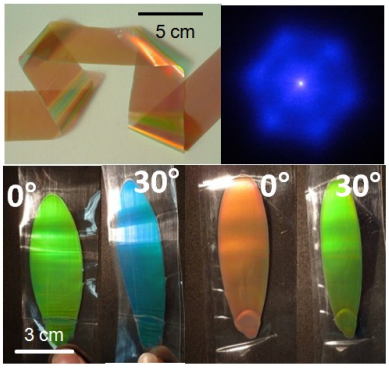

Supporting Information should be included here (for submission only; for publication, please provide Supporting Information as a separate PDF file).

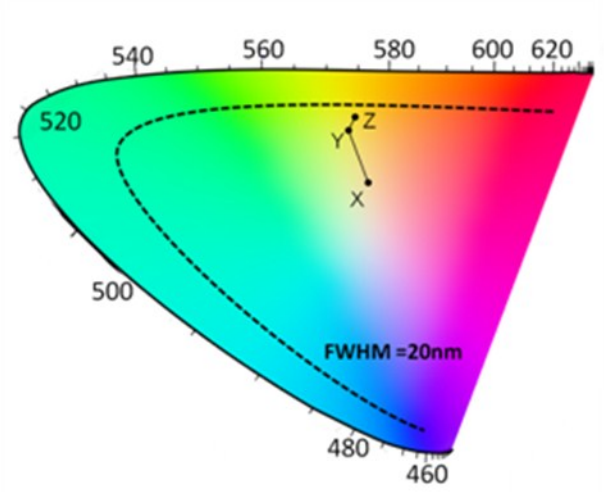

Figure S1. Chromaticity CIE colors from bright-field spectra, of edge-sheared (single-pass, point Y; 3 passes, Z) and pre-sheared (point X) samples. Dashed line shows locus of colors with 20nm spectral bandwidth.

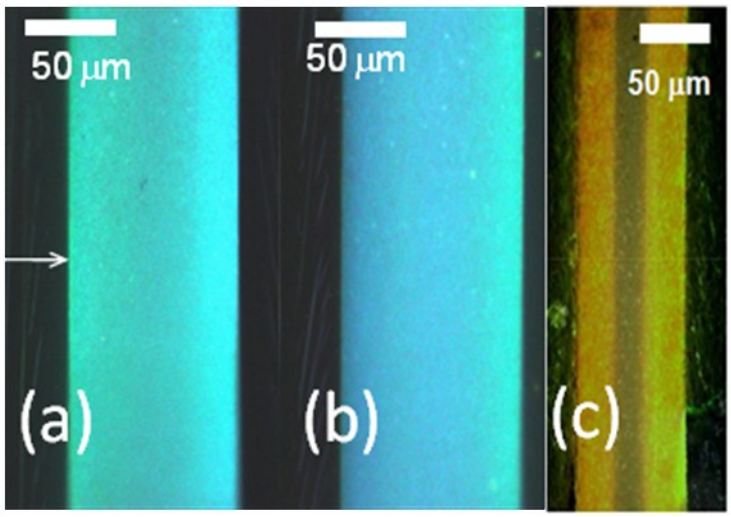

Figure S2. Microscope image (x20, dark-field) of green-opal film in cross-section transverse to the edge-shear processing direction, (a) after, and (b) before edge-shear process. In (a), the lower face of the film touching the hot-edge is shown by arrow. (c) Comparison sample prepared by compressive shear, showing ordered outer layers.

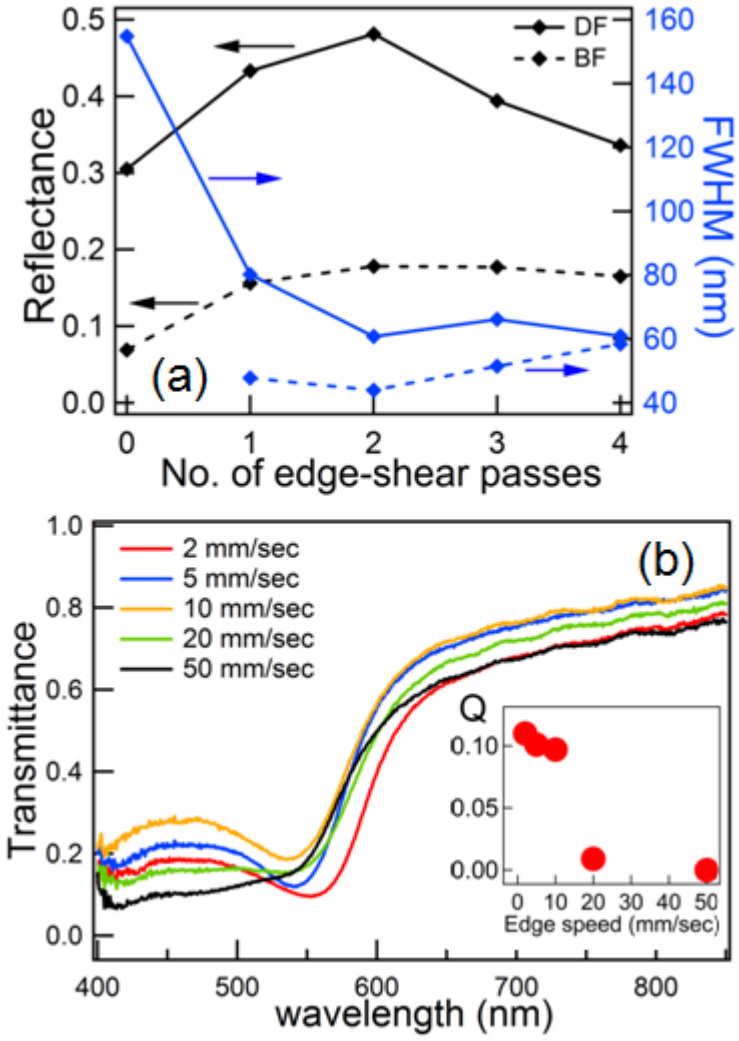

Figure S3. (a) Maximum reflectance and resonance linewidth for dark-field (solid) and bright-field (dashed) vs number of edge-shear passes. (b) Transmission of green opaline films vs single-pass edge-shearing speed. Inset; sample quality, *Q*, (see text) vs edge pass speed.